Inorganic Chemistry

Article

pubs.acs.org/IC

Thiazyl Trifluoride (NSF_3) Adducts and Imidodifluorosulfate (F_2OSN-) Derivatives of $Hg(OTeF_5)_2$

John R. DeBackere, Hélène P. A. Mercier, and Gary J. Schrobilgen*

Department of Chemistry, McMaster University, Hamilton, Ontario L8S 4M1, Canada

Supporting Information

ABSTRACT: Reactions of $Hg(OTeF_5)_2$ with excess amounts of NSF_3 at 0 °C result in the formation of NSF_3 adducts having the compositions $[Hg(OTeF_5)_2{\cdot}N{\equiv}SF_3]_\infty$ (**1**), $[Hg(OTeF_5)_2{\cdot}2N{\equiv}SF_3]_2$ (**2**), and $Hg_3(OTeF_5)_6{\cdot}4N{\equiv}SF_3$ (**3**). When the reactions are carried out at room temperature, oxygen/fluorine metatheses occur yielding the F_2OSN- derivatives $[Hg(OTeF_5)(N{=}SOF_2){\cdot}N{\equiv}SF_3]_\infty$ (**4**) and $[Hg_3(OTeF_5)_5(N{=}SOF_2){\cdot}2N{\equiv}SF_3]_2$ (**5**). The proposed reaction pathway leading to F_2OSN- group formation occurs by nucleophilic attack by a F_5TeO- group at the sulfur(VI) atom of NSF_3, followed by TeF_6 elimination. Tellurium hexafluoride formation was confirmed by ^{19}F NMR spectroscopy. The NSF_3 molecules are terminally N-coordinated to mercury, whereas the F_2OSN- ligands are N-bridged to two mercury atoms. The compound series was characterized by low-temperature single-crystal X-ray diffraction and low-temperature Raman spectroscopy. Several structural motifs are observed within this structurally diverse series. These include the infinite chain structures of the related compounds, **1** and **4**; **2**, a dimeric structure which possesses an $(HgO_\mu)_2$ ring at its core; **3**, a structure based on a cage comprised of a $(HgO_\mu)_3$ ring that is capped on each face by μ^3-oxygen bridged F_5TeO- groups; and **5**, a dimeric structure possessing two distorted (Hg_3O_2N) rings that are formally derived from **3** by replacement of a F_5TeO- group by a F_2OSN- group in each ring. Quantum-chemical calculations were carried out to gain insight into the bonding of the μ^3-oxygen bridged teflate groups observed in structure **3**. Compounds **1**−**5** represent a novel class of neutral transition metal complexes with NSF_3, providing the first examples of NSF_3 coordination to mercury. Compounds **4** and **5** also provide the only examples of F_2OSN- derivatives of mercury that have been characterized by single-crystal X-ray diffraction.

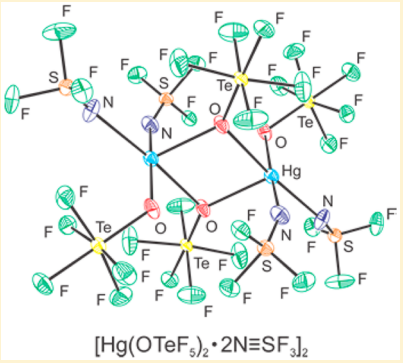

INTRODUCTION

Thiazyl trifluoride, NSF_3, has been of importance as a synthetic precursor and in the development of sulfur−nitrogen−fluorine chemistry.[1−4] The distorted tetrahedral geometry of NSF_3 has been thoroughly studied by ^{19}F NMR,[5] IR,[5−7] Raman,[8] microwave spectroscopy,[9] and by low-temperature single-crystal X-ray diffraction.[10] The reactivity of NSF_3 may be categorized into three reaction types: (1) addition to the π-system of the N≡S bond, (2) nucleophilic attack at the positively charged and coordinatively unsaturated sulfur(VI) atom, and (3) donation of the nitrogen electron lone pair to a Lewis acidic center.

The Lewis basicity of NSF_3 is illustrated by its reactions with the Lewis acids AsF_5, SbF_5, and BF_3, which yield the Lewis acid−base adducts $F_3S{\equiv}NAsF_5$,[3,11] $F_3S{\equiv}NSbF_5$,[11] and $F_3S{\equiv}NBF_3$.[6,12] Other NSF_3 adducts with main-group atom centers include $[(CF_3)_nSF_{3-n}N{\equiv}SF_3][AsF_6]$ (n = 0−2),[13] $[F_3S(N{\equiv}SF_3)_2][AsF_6]$,[14] $[F_4SNXeN{\equiv}SF_3][AsF_6]$,[14] and $[F_3S{\equiv}NXeF][AsF_6]$,[15] with the latter three adduct-cations and $F_3S{\equiv}NAsF_5$,[3] having been characterized by single-crystal X-ray diffraction. The reactions of NSF_3 with Lewis acidic metal centers have also been studied and provide a series of transition metal adducts $[M(N{\equiv}SF_3)_4][AsF_6]_2$ (M = Mn, Fe, Co, Ni, Cu, Zn),[16−18] $[CpFe(CO)_2N{\equiv}SF_3][AsF_6]$,[19] $[M(CO)_5N{\equiv}SF_3][AsF_6]$ (M = Mn, Re),[19,20] and $[Ag(N{\equiv}SF_3)_n][AsF_6]$ (n = 1, 2),[16] which have been structurally characterized by physical methods such as IR and/or Raman spectroscopy, NMR spectroscopy, and mass spectrometry. The only transition metal complexes of NSF_3 that have been characterized by single-crystal X-ray diffraction are $[M(N{\equiv}SF_3)_4][AsF_6]_2$ (M = Mn,[17] Zn[18]), $[Re(CO)_5N{\equiv}SF_3][AsF_6]$,[19] and $[CpFe(CO)_2N{\equiv}SF_3][AsF_6]$.[19] The NSF_3 ligands of these complexes are terminally N-coordinated to the metal.

A considerable number of covalently bonded main-group derivatives of the F_2OSN- ligand are known as exemplified by $XNSOF_2$ (X = H, F, Cl, Br, I, $(CH_3)_3Si$, $CH_3OS(O)$, CF_3CO, CF_3S, $OCNSO_2$, Cl_3PNSO_2, OCNCO, $(C_6H_5)_4As$, $(C_6H_5)_4P$, $O{=}PF_2$, $O{=}PFCl$, $O{=}PCl_2$, $S{=}PCl_2$, $(CH_3)_2SnCl$, $(CH_3)_2SnBr$),[21−25] $X(NSOF_2)_2$ (X = $(CH_3)_2Si$, $(C_6H_5)CH_3Si$, OS, OSe, O_2S, $O{=}PF$, $O{=}PCl$, $S{=}PCl$, $S{=}PF$, $(CH_3)_2Sn$),[22−25] $X(NSOF_2)_3$ (X = B, P, As, Sb, CH_3Si, $O{=}P$, $S{=}P$),[22−25] $(N{=}CNSOF_2)_3$,[26] $[B(NSOF_2)_4]^-$,[27] $Si(NSOF_2)_4$,[22] and $Sb(NSOF_2)_5$.[22,24] Examples of transition metal derivatives include $Hg(NSOF_2)_2$,[21] $AgNSOF_2$,[25] $Re(CO)_5(NSOF_2)$,[28] $[(CO)_4M(NSOF_2)]_2$ (M = Re,[28] Mn[28−30]), $M(NSOF_2)_2$ (M = Ni, Co, Cu),[31] $Cu(NSOF_2)(AsF_5NSOF_2)$,[31] $[Ni(SO_2)_2][AsF_4(NSOF_2)]_2$,[31] as well as the $[Ag(NSOF_2)_2]^-$[32]

Received: August 4, 2015
Published: September 28, 2015

DOI: 10.1021/acs.inorgchem.5b01769
Inorg. Chem. 2015, 54, 9989−10000

and $[M(NSOF_2)_4]^{2-}$ anions (M = Zn, Hg, Mn, Co, Pd, Cu).[32,33] Their structural characterizations have been limited to IR and/or Raman spectroscopy, NMR spectroscopy, electron diffraction, and mass spectrometry. The only F_2OSN- derivatives that have been characterized by single-crystal X-ray diffraction are $(NCNSOF_2)_3$,[26] $[Ni(SO_2)_2]$-$[AsF_4(NSOF_2)_2]_2$,[31] and $[(CO)_4Mn(NSOF_2)]_2$.[29,30] In the case of $(NCNSOF_2)_3$, the trimeric structure is comprised of an *s*-C_3N_3 ring in which the F_2OSN- groups are bonded to carbon.[26] The F_2OSN- ligands of the transition metal derivatives bridge two metal centers.

The X-ray crystal structure of $Hg(OTeF_5)_2$ consists of discrete $Hg(OTeF_5)_2$ units that interact through long Hg---O and Hg---F intermolecular contacts.[34] The Lewis acidity of $Hg(OTeF_5)_2$ was recently demonstrated by the syntheses of the noble-gas difluoride adducts, $Hg(OTeF_5)_2 \cdot 1.5NgF_2$ (Ng = Kr or Xe)[34] and a series of mercury(II) pentafluoro-oxotellurate-(VI) anions.[35] The bulky, highly electronegative F_5TeO- (teflate) group is terminally bonded in the majority of its compounds. However, several examples of μ-oxygen bonded F_5TeO- groups are known, e.g., $Au(OTeF_5)_3$,[36] $[AgOTeF_5$-$(C_6H_5Cl)_3)_2]_2$,[37] $[AgOTeF_5(1,2\text{-}C_2H_4Cl_2)]_2$,[38,39] $[Zn$-$(OTeF_5)_2(C_6H_5NO_2)_2]_2$,[40] $[Ag(CO)][B(OTeF_5)_4]$,[41] and Ag-$(CH_2Cl_2)Pd(OTeF_5)_4$.[39,42] Oxygen-bridged F_5TeO- ligands have also been observed for several Hg(II) teflate salts, $[N(CH_3)_4]_2[Hg_2(OTeF_5)_6]$, $Cs_2[Hg(OTeF_5)_4] \cdot Hg(OTeF_5)_2$, and $\{Cs_3[Hg_2(OTeF_5)_7] \cdot Hg(OTeF_5)_2\} \cdot 4SO_2ClF$.

In view of the limited number of metal NSF_3 adducts that have been structurally characterized, and the absence of NSF_3 coordination complexes of mercury, the possible formation of NSF_3 adducts with $Hg(OTeF_5)_2$ and their structures were of interest. Prior to this study, the known transition metal complexes of NSF_3 had been limited to cations that were stabilized by the weakly fluoro-basic $[AsF_6]^-$ anion. The present study describes the reactivity of $Hg(OTeF_5)_2$ with NSF_3 and the formation and structural characterization of several neutral NSF_3 adducts and structurally related compounds that contain F_2OSN- groups.

RESULTS AND DISCUSSION

Syntheses. The compounds $[Hg(OTeF_5)_2 \cdot N{\equiv}SF_3]_\infty$, $[Hg(OTeF_5)_2 \cdot 2N{\equiv}SF_3]_2$, and $Hg_3(OTeF_5)_6 \cdot 4N{\equiv}SF_3$ were synthesized by the reaction of $Hg(OTeF_5)_2$ with NSF_3 at 0 °C in their respective solvents (see Experimental Section). Reactions carried out at 0 °C formed mixtures of NSF_3 adducts (see Experimental Section), whereas reactions carried out at room temperature over periods of several hours resulted in F/O metatheses, yielding the mixed NSF_3/F_2OSN- derivatives, $[Hg(OTeF_5)(N{=}SOF_2) \cdot N{\equiv}SF_3]_\infty$ and $[Hg_3(OTeF_5)_5(N{=}SOF_2) \cdot 2N{\equiv}SF_3]_2$. These observations were supported by Raman spectroscopy which showed the absence of F_2OSN- ligand stretching bands when reaction mixtures were not warmed above 0 °C for extended periods of time. However, when these reactions were carried out at room temperature in SO_2ClF and rapidly crystallized (within ca. 3 h), only $Hg_3(OTeF_5)_6 \cdot 4N{\equiv}SF_3$ was isolated. Low-temperature Raman spectra were recorded on the colorless crystalline products that were obtained by slow solvent evaporation. The Raman spectra, in conjunction with unit cell determinations, were used to speciate the reaction mixtures.

A proposed reaction pathway for the formation of the F_2OSN- group is provided in Scheme 1. The stable coordination compounds $[Hg(OTeF_5)_2 \cdot N{\equiv}SF_3]_\infty$, $[Hg$-$(OTeF_5)_2 \cdot 2N{\equiv}SF_3]_2$, and $[Hg_3(OTeF_5)_6 \cdot 4N{\equiv}SF_3]$ are initially formed at 0 °C (eq 1). At room temperature, nucleophilic attack by a F_5TeO- group occurs at sulfur (eq 2) to form the $(F_5TeO)F_3S{=}N$- ligand as an intermediate. The related $F_4S{=}N$ group was characterized by single-crystal X-ray diffraction in $[F_4S{=}NXe][AsF_6]$.[43] Subsequent elimination of gaseous TeF_6 from the intermediate, $(F_5TeO)Hg\{N{=}SF_3(OTeF_5)\}$, at room temperature leads to F_2OSN- group formation (eq 3). The formation of TeF_6 in Scheme 1 was confirmed by ^{19}F NMR spectroscopy for the reaction of $Hg(OTeF_5)_2$ with excess NSF_3 in Freon-114 (1,2-dichlorotetrafluoroethane) solvent. After reaction at room temperature for 24 h, the volatile components of the reaction mixture were isolated by vacuum distillation and their ^{19}F NMR spectrum was recorded. The spectrum consisted of intense resonances due to TeF_6 [−53.7 ppm, $^1J(^{125}Te{-}^{19}F)$ = 3738 Hz, $^1J(^{123}Te{-}^{19}F)$ = 3100 Hz], unreacted NSF_3 [67.9 ppm, $^2J(^{19}F{-}^{14}N)$ = 25.9 Hz], and Freon-114 (−72.4 ppm). The NMR parameters of TeF_6 are in good agreement with previously reported values.[44] Several very low-intensity AB_4 patterns assigned to F_5TeO- groups were also observed between −33 and −54 ppm.

Scheme 1. Proposed Reaction Pathway for the O/F Metatheses of $Hg(OTeF_5)_2$ Adducts of NSF_3

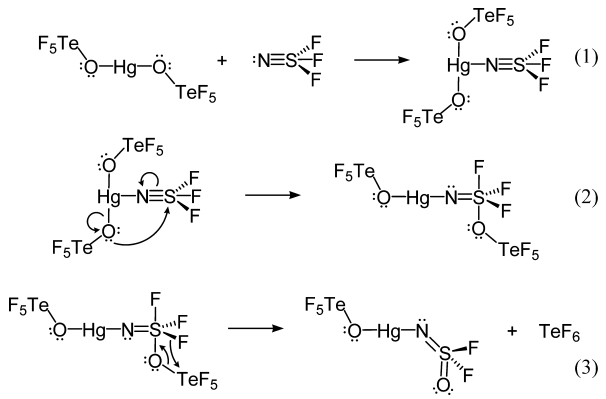

The reaction of $Hg(OTeF_5)_2$ with NSF_3 at room temperature for 11 days in Freon-114 only yielded $[Hg(OTeF_5)(N{=}SOF_2) \cdot N{\equiv}SF_3]_\infty$, with no sign of nucleophilic attack of NSF_3 by the remaining F_5TeO- group.

X-ray Crystallography. Summaries of the data collection parameters and other crystallographic information for $[Hg(OTeF_5)_2 \cdot N{\equiv}SF_3]_\infty$ (**1**), $[Hg(OTeF_5)_2 \cdot 2N{\equiv}SF_3]_2$ (**2**), $Hg_3(OTeF_5)_6 \cdot 4N{\equiv}SF_3$ (**3**), $[Hg(OTeF_5)(N{=}SOF_2) \cdot N{\equiv}SF_3]_\infty$ (**4**), and $[Hg_3(OTeF_5)_5(N{=}SOF_2) \cdot 2N{\equiv}SF_3]_2$ (**5**) are provided in Table 1. Selected bond lengths and bond angles are provided in Tables 2−6, and full lists of geometrical parameters are given in Tables S1−S6. In cases where F_5TeO- groups and NSF_3 are affected by disorder (see Experimental Section, X-ray Crystallography), only the geometrical parameters of the ordered groups are discussed. The geometrical parameters associated with the F_5TeO- groups are in good agreement with previously published values[34,35] and do not require further commentary.

(a) $[Hg(OTeF_5)_2 \cdot N{\equiv}SF_3]_\infty$. The crystal structure of $[Hg(OTeF_5)_2 \cdot N{\equiv}SF_3]_\infty$ (Figure 1) consists of well-isolated chains which run parallel to the *a*-axis of the crystallographic unit cell. The chains interact with one another through weak F---F intermolecular contacts (2.75(6)−2.94(8) Å) that are close to twice the F van der Waals radius (2 × 1.47 Å).[45] The repeat unit of the chain consists of a $Hg(OTeF_5)_2$ molecule that is N-

DOI: 10.1021/acs.inorgchem.5b01769
Inorg. Chem. 2015, 54, 9989−10000

Table 1. Summaries of Crystal Data and Refinement Results for $[Hg(OTeF_5)_2{\cdot}N{\equiv}SF_3]_\infty$ (1), $[Hg(OTeF_5)_2{\cdot}2N{\equiv}SF_3]_2$ (2), $Hg_3(OTeF_5)_6{\cdot}4N{\equiv}SF_3$ (3), $[Hg(OTeF_5)(N{=}SOF_2){\cdot}N{\equiv}SF_3]_\infty$ (4), and $[Hg_3(OTeF_5)_5(N{=}SOF_2){\cdot}2N{\equiv}SF_3]_2$ (5)

compound	1	2	3	4	5
space group	$P2_1/n$	$P2_1/c$	$Pna2_1$	$P2_1/c$	$P\bar{1}$
a (Å)	6.6574(2)	8.295(2)	24.1661(15)	9.4117(6)	10.2252(11)
b (Å)	11.7945(4)	10.489(2)	13.7016(10)	21.6140(15)	10.9529(11)
c (Å)	15.5201(5)	17.853(4)	12.8714(8)	17.3578(12)	17.5285(19)
α (deg)	90.0	90.0	90.0	90.0	103.114(6)
β (deg)	94.305(2)	95.887(4)	90.0	104.116(1)	93.788(6)
γ (deg)	90.0	90.0	90.0	90.0	116.496(5)
V (Å^3)	1215.21(7)	1545.2(6)	4261.9(5)	3424.4(4)	1679.3(3)
molecules/unit cell	4	2	4	12	1
mol wt (g mol^{-1})	780.86	883.93	2445.65	642.33	2100.98
calcd density (g cm^{-3})	4.268	3.800	3.812	3.738	4.155
T (°C)	−173	−173	−173	−173	−173
μ (mm^{-1})	17.71	14.112	15.22	16.49	18.34
R_1[a]	0.0307	0.0568	0.0387	0.0250	0.0502
wR_2[b]	0.0563	0.1093	0.0849	0.0519	0.1140

[a] R_1 is defined as $\Sigma||F_0| - |F_c||/\Sigma|F_0|$ for $I > 2\sigma(I)$. [b] wR_2 is defined as $[\Sigma[w(F_0^2 - F_c^2)^2]/\Sigma w(F_0^2)^2]^{1/2}$ for $I > 2\sigma(I)$.

Table 2. Selected Experimental Geometrical Parameters for $[Hg(OTeF_5)_2{\cdot}N{\equiv}SF_3]_\infty$[a]

	Bond Lengths (Å)		
$Hg_1{-}O_1$	2.241(4)	Te−O	1.811(5)−1.812(4)
$Hg_1{-}O_2$	2.227(5)	Te−F	1.823(6)−1.871(5)
$Hg_1{-}O_{1A}$	2.502(4)		
$Hg_1{-}O_{2B}$	2.470(4)	N−S	1.398(5)
$Hg_1{-}N_1$	2.112(5)	S−F	1.489(6)−1.516(7)
	Bond Angles (deg)		
$O_1{-}Hg_1{-}O_2$	84.5(2)	$O_1{-}Hg_1{-}O_{1A}$	76.5(2)
$N_1{-}Hg_1{-}O_1$	134.5(2)	$O_1{-}Hg_1{-}O_{2B}$	108.0(2)
$N_1{-}Hg_1{-}O_2$	140.9(2)	$O_2{-}Hg_1{-}O_{1A}$	99.6(2)
$N_1{-}Hg_1{-}O_{1A}$	92.1(2)	$O_2{-}Hg_1{-}O_{2B}$	75.4(2)
$N_1{-}Hg_1{-}O_{2B}$	88.7(2)	$O_{1A}{-}Hg_1{-}O_{2B}$	172.6(2)
$Hg_1{-}N_1{-}S_1$	160.5(4)		
N−S−F	119.3(6)−128(3)	F−S−F	95.4(8)−96.5(7)

[a] The atom labeling scheme corresponds to that used in Figure 1. See Table S1 for a complete list of geometrical parameters.

Table 3. Selected Experimental Geometrical Parameters for $[Hg(OTeF_5)_2{\cdot}2N{\equiv}SF_3]_2$[a]

	Bond Lengths (Å)		
$Hg_1{-}O_1$	2.154(8)	Te−O	1.798(7)−1.820(8)
$Hg_1{-}O_2$	2.348(7)	Te−F	1.820(8)−1.858(7)
$Hg_1{-}O_{2A}$	2.467(8)		
$Hg_1{-}N_1$	2.164(10)	N−S	1.388(10)−1.394(10)
$Hg_1{-}N_2$	2.377(10)	S−F	1.498(7)−1.544(7)
	Bond Angles (deg)		
$O_1{-}Hg_1{-}O_2$	94.0(3)	$Hg_1{-}O_2{-}Hg_{1A}$	100.8(3)
$O_1{-}Hg_1{-}O_{2A}$	86.4(3)	$Hg_1{-}N_1{-}S_1$	154.7(7)
$O_1{-}Hg_1{-}N_1$	169.3(4)	$Hg_1{-}N_2{-}S_2$	150.8(6)
$O_1{-}Hg_1{-}N_2$	94.4(3)	$N_1{-}Hg_1{-}N_2$	93.3(4)
$O_2{-}Hg_1{-}O_{2A}$	79.2(3)	$N_1{-}Hg_1{-}O_{2A}$	85.4(3)
$O_2{-}Hg_1{-}N_1$	91.2(3)	$N_2{-}Hg_1{-}O_{2A}$	174.8(3)
$O_2{-}Hg_1{-}N_2$	105.9(3)		
N−S−F	119.3(6)−123.1(6)	F−S−F	94.3(4)−96.6(4)

[a] The atom labeling scheme corresponds to that used in Figure 2. See Table S2 for a complete list of geometrical parameters.

coordinated to an NSF_3 molecule (Figure 1). The coordination sphere of each mercury atom is comprised of four bridging F_5TeO- groups ($Hg_{(1)}{-}O_{(2)}$, 2.227(5) Å; $Hg_{(1)}{-}O_{(1)}$, 2.241(4) Å; $Hg_{(1)}{-}O_{(1A)}$, 2.470(4) Å; $Hg_{(1)}{-}O_{(2B)}$, 2.502(4) Å), two of them being symmetry related, and a terminal NSF_3 group (Hg−N, 2.122(5) Å). The ligand atom arrangements around each five-coordinate mercury atom lie between a square pyramid and a trigonal bipyramid as indicated by the τ-parameter,[46] 0.548, where $\tau = |\beta - \alpha|/60$ and β and α are the two largest coordination angles involving different ligand atoms in the mercury coordination sphere. The ideal values for a square pyramid and a trigonal bipyramid are 0 and 1,

DOI: 10.1021/acs.inorgchem.5b01769
Inorg. Chem. 2015, 54, 9989−10000

Table 4. Selected Experimental Geometrical Parameters for $Hg_3(OTeF_5)_6 \cdot 4N{\equiv}SF_3$[a]

		Bond Lengths (Å)	
Hg_1-O_1	2.327(8)	Hg_3-O_1	2.644(7)
$Hg_1\cdots O_2$	2.781(11)	$Hg_3\cdots O_2$	2.723(11)
Hg_1-O_5	2.307(10)	Hg_3-O_3	2.192(9)
Hg_1-O_4	2.301(8)	Hg_3-O_4	2.292(8)
Hg_1-N_1	2.265(11)	Hg_3-N_2	2.234(11)
Hg_1-N_4	2.223(10)	Hg_3-N_3	2.240(11)
Hg_2-O_1	2.501(8)	Te−O	1.787(8)−1.836(7)
Hg_2-O_2	2.143(7)	Te−F	1.806(10)−1.860(10)
Hg_2-O_3	2.501(8)		
Hg_2-O_5	2.557(9)	N−S	1.371(11) −1.398 (11)
Hg_2-O_6	2.051(9)	S−F	1.506(5)−1.536(7)
		Bond Angles (deg)	
$Hg_1-O_1-Hg_2$	96.2(4)	$O_5-Hg_2-O_3$	136.3(4)
$Hg_1-O_1-Hg_3$	95.7(4)	$O_5-Hg_2-O_1$	70.2(4)
$Hg_2-O_1-Hg_3$	90.0(3)	$O_5-Hg_2-O_2$	75.8(4)
$Hg_1-O_2-Hg_2$	92.9(4)	$O_3-Hg_2-O_1$	70.0(4)
$Hg_1-O_2-Hg_3$	84.2(3)	$O_3-Hg_2-O_2$	76.0(4)
$Hg_2-O_2-Hg_3$	96.0(4)	$O_1-Hg_2-O_2$	73.1(4)
$Hg_1-O_4-Hg_3$	107.0(4)	$O_2-Hg_3-O_3$	70.6(4)
$Hg_3-O_3-Hg_2$	101.4(5)	$O_2-Hg_3-O_4$	73.2(4)
$Hg_2-O_5-Hg_1$	95.1(4)	$O_2-Hg_3-O_1$	62.4(3)
$N_1-Hg_1-N_4$	94.3(7)	$O_3-Hg_3-O_4$	136.6(4)
$N_2-Hg_3-N_3$	108.7(6)	$O_3-Hg_3-O_1$	72.1(4)
$O_5-Hg_1-O_1$	77.8(4)	$O_4-Hg_3-O_1$	70.4(4)
$O_5-Hg_1-O_2$	69.0(4)	$O_1-Hg_1-O_4$	76.3(4)
$O_5-Hg_1-O_4$	139.4(4)	$O_2-Hg_1-O_4$	71.9(3)
$O_1-Hg_1-O_2$	65.2(3)		
$Hg_1-N_1-S_1$	151(1)	$Hg_3-N_3-S_3$	166(1)
$Hg_1-N_4-S_4$	176(1)	$Hg_3-N_2-S_2$	161(1)
N−S−F	116.3(12)−126.4(12)	F−S−F	93.5(8)−98.0(8)
		Dihedral Angle (deg)	
$Te_6-O_6-Hg_2-O_2-Te_2$		5.8 (8)	

[a]The atom labeling scheme corresponds to that used in Figure 3. See Table S3 for a complete list of geometrical parameters.

respectively. The Hg−O bond lengths are longer than those of $Hg(OTeF_5)_2$ (2.016(6) Å). Bond elongations presumably result from electron density donated to the Lewis-acidic mercury center by the nitrogen lone pair of NSF_3 which, in turn, diminishes the covalent characters of the Hg−O bonds. This is also reflected in the Te−O bond lengths, which are shorter (1.798(2)−1.802(2) Å) than the Te−O bonds of $Hg(OTeF_5)_2$ (1.842(7) Å), and is consistent with enhancement of the π characters of their Te−O bonds.[35] The Te−O bond lengths of $[Hg(OTeF_5)_2 \cdot N{\equiv}SF_3]_\infty$ are comparable to the Te−O_μ bond lengths of $[Hg_2(OTeF_5)_6]^{2-}$ (1.790(4) and 1.802(4) Å).[35] The $O_{(1A)}-Hg_{(1)}-O_{(2B)}$ angle (172.6(2)°) is comparable to that of $Hg(OTeF_5)_2$ (170.5(4)°) in its crystal structure,[34] which also exhibits a *gauche*-conformation. The Hg−N bond length (2.122(5) Å) is similar to those of $Hg(NSF_2)_2$ (2.050(13) Å)[47] and $[Hg(N_3)_3]^-$ (2.077(4)−2.113(2) Å).[48] The Hg−N−S angle is bent (160.5(4)°), as previously observed in $[Mn(N{\equiv}SF_3)_4][AsF_6]_2$ (162.0(3)°),[17] and is significantly less than the ideal 180° angle observed in $F_5AsN{\equiv}SF_3$,[3] suggesting that intra- and/or intermolecular contacts within the crystal lattice may be responsible for the bent angle. An even more severely bent angle occurs in $[F_3S{\equiv}NXeF][AsF_6]$ (∠Xe−N−S, 142.6(3)°), whereas quantum-chemical calculations predict a linear structure, thus supporting the influence of crystal packing on the Xe−N−S angle,[15] and by inference, on the Hg−N−S angle.

The S−F (1.489(6)−1.516(7) Å) bond lengths are comparable to those of $[M(N{\equiv}SF_3)_4][AsF_6]_2$ (Mn, 1.501(5)−1.511(4) Å; Zn, 1.423(9)−1.515(5) Å),[17,18] $[Re(CO)_5N{\equiv}SF_3][AsF_6]$ (1.499(10) Å),[19] and $[CpFe(CO)_2N{\equiv}SF_3][AsF_6]$ (1.512(3)−1.519(3) Å).[19] The shorter S−F bond lengths of adducted NSF_3 relative to those of free NSF_3 (1.531(1)−1.534(2) Å) are consistent with adduct formation.[10] The N−S bond lengths (1.398(5) Å) are also comparable to those of $[M(N{\equiv}SF_3)_4][AsF_6]_2$ (Mn, 1.357(6)−1.373(5) Å; Zn, 1.350(7)−1.387(6) Å), $[Re(CO)_5N{\equiv}SF_3][AsF_6]$ (1.384(14) Å), $[CpFe(CO)_2N{\equiv}SF_3][AsF_6]$ (1.376(3) Å), and free NSF_3 (1.400(3) Å). The N−S−F (119.3(6)−121.8(6)°) and F−S−F (95.6(5)−96.5(4)°) bond angles are similar to those of the metal complexes and free NSF_3 and require no further commentary.

(b) $[Hg(OTeF_5)_2 \cdot 2N{\equiv}SF_3]_2$. The crystal structure of $[Hg(OTeF_5)_2 \cdot 2N{\equiv}SF_3]_2$ (Figure 2) consists of well-isolated dimers with the shortest intermolecular F---F distances (2.732(11)−2.930(12) Å) being close to the sum of twice the F van der Waals radius (2.94 Å). The mercury coordination spheres are comprised of a terminal F_5TeO- group (Hg−O, 2.154(8) Å), two bridging F_5TeO_μ groups (Hg−O_μ, 2.348(7), 2.467(8) Å), and two N-coordinated NSF_3 molecules (Hg−N, 2.164(10), 2.377(10) Å). Aspects of this structure are similar to those of the dimeric $[Hg_2(OTeF_5)_6]^{2-}$ anion, which has slightly shorter Hg−O (2.040(4)−2.104(5) Å) and comparable Hg−

DOI: 10.1021/acs.inorgchem.5b01769
Inorg. Chem. 2015, 54, 9989−10000

Table 5. Selected Experimental Geometrical Parameters for $[Hg(OTeF_5)(N{=}SOF_2)\cdot N{\equiv}SF_3]_\infty$[a]

Bond Lengths (Å)			
Hg_1-O_1	2.537(2)	Hg_3-O_3	2.483(2)
Hg_1-O_{3A}	2.408(2)	Hg_3-O_2	2.425(2)
Hg_1-N_1	2.130(2)	Hg_3-N_5	2.130(2)
Hg_1-N_{5A}	2.146(2)	Hg_3-N_4	2.156(2)
Hg_1-N_2	2.496(3)	$Hg_3\cdots N_6$	2.538(3)
Hg_2-O_1	2.415(2)	$Hg_2\cdots N_3$	2.573(3)
Hg_2-N_1	2.127(2)	Hg_2-N_4	2.109(2)
Te−O	1.798(2)−1.802(2)	Hg_2-O_2	2.506(2)
Te−F	1.838(2)−1.864(2)		
F_2OSN- group		NSF_3	
N−S	1.484(2)−1.487(2)	N−S	1.399(3)−1.407(3)
S−O	1.403(3)−1.407(2)	S−F	1.519(3)−1.533(2)
S−F	1.525(2)−1.540(2)		
Bond Angles (deg)			
$Hg_1-O_1-Hg_2$	91.8(1)	$N_1-Hg_2-O_1$	78.5(1)
$Hg_1-N_1-Hg_2$	113.4(1)	$O_2-Hg_2-N_4$	77.8(1)
$Hg_2-O_2-Hg_3$	91.6(1)	$N_4-Hg_3-O_2$	78.7(1)
$Hg_2-N_4-Hg_3$	111.9(1)	$N_5-Hg_3-O_3$	76.1(1)
$Hg_3-O_3-Hg_{1A}$	56.7(1)	$N_{5A}-Hg_1-O_{3A}$	77.4(1)
$Hg_3-N_5-Hg_{1A}$	89.6(1)	$N_1-Hg_1-O_1$	75.7(1)
$S_1-N_1-Hg_1$	122.2(1)	$S_4-N_4-Hg_2$	126.8(1)
$S_1-N_1-Hg_2$	124.4(1)	$S_4-N_4-Hg_3$	121.3(1)
$S_5-N_5-Hg_3$	124.5(1)	$S_5-N_5-Hg_{1A}$	123.6(1)
F_2OSN- group		NSF_3	
N−S−O	122.1(2)−123.2(1)	N−S−F	120.0(2)−122.8(2)
N−S−F	108.5(1)−110.6(1)	F−S−F	94.9(1)−95.9(1)
O−S−F	107.1(2)−109.1(1)		
F−S−F	93.7(1)−94.7(1)		

[a]The atom labeling scheme corresponds to that used in Figure 4. See Table S4 for a complete list of geometrical parameters.

O_μ (2.350(4)−2.508(4) Å) bond lengths.[35] In the present instance, the dimeric structure is generated through an inversion center; i.e., the adduct is comprised of two crystallographically equivalent $Hg(OTeF_5)_2(N{\equiv}SF_3)_2$ moieties that are coordinated to one another through two bridging F_5TeO_μ groups. As observed in $[Hg_2(OTeF_5)_6]^{2-}$, the O_μ atoms and the two Hg atoms form a $(HgO_\mu)_2$ ring. The $Hg-O_\mu-Hg$ (100.8(3)°) and $O_\mu-Hg-O_\mu$ (79.2(3)°) bridge angles are comparable to those of $[Hg_2(OTeF_5)_6]^{2-}$ ($\angle Hg-O_\mu-Hg$, 102.1(1)°, 104.6(1)°; $\angle O_\mu-Hg-O_\mu$, 70.1(1)°, 73.9(1)°).[35] The τ-parameter, 0.092, associated with the Hg coordination sphere is close to that of a square pyramid (see above). The $O_{(2)}$ atom occupies the axial position, whereas the remaining ligand atoms ($O_{(2A)}$, $O_{(1)}$, $N_{(1)}$, and $N_{(2)}$) occupy the equatorial positions of the square pyramid.

The coordinated NSF_3 molecules possess N−S (1.388(10), 1.394(10) Å) and S−F (1.498(7)−1.544(7) Å) bond lengths, as well as $\angle N-S-F$ (119.3(6)−123.1(6)°) and $\angle F-S-F$ (94.3(4)−96.6(4)°) bond angles that are comparable to those of $[Hg(OTeF_5)_2\cdot N{\equiv}SF_3]_\infty$ (see above). The more weakly coordinated NSF_3 ligands (Hg_1-N_2, 2.377(10) Å) lie in the plane of the $(HgO_\mu)_2$ ring, whereas the more strongly bonded NSF_3 ligands ($Hg_{(1)}-N_{(1)}$, 2.164(10) Å) are perpendicular to the $(HgO_\mu)_2$ ring and lie on either side of it. The Hg−N−S angles (150.8(6), 154.7(7)°) are more closed than those of $[Hg(OTeF_5)_2\cdot N{\equiv}SF_3]_\infty$.

(c) $Hg_3(OTeF_5)_6\cdot 4N{\equiv}SF_3$. The crystal structure of $Hg_3(OTeF_5)_6\cdot 4N{\equiv}SF_3$ (Figure 3) consists of a well-isolated structural unit, with the shortest intermolecular F---F distances ranging from 2.68(3) to 2.94(2) Å, close to twice the sum of the fluorine van der Waals radii.[45,49] The structure may be formally described as the interaction of a $Hg_{(2)}(OTeF_5)_2$ molecule with $[Hg(OTeF_5)_2\cdot 2N{\equiv}SF_3]_2$. The oxygen atoms of the $F_5TeO_{(3,5)}$ groups of $[Hg(OTeF_5)_2\cdot 2N{\equiv}SF_3]_2$ behave as pincers in their coordination to $Hg_{(2)}$ ($Hg_{(2)}-O_{(3)}$, 2.501(8) Å; $Hg_{(2)}-O_{(5)}$, 2.557(9) Å), whereas the $F_5TeO_{(1)}$ group of $[Hg(OTeF_5)_2\cdot 2N{\equiv}SF_3]_2$ interacts with $Hg_{(2)}(OTeF_5)_2$ through a short $Hg_{(2)}-O_{(1)}$ contact (2.501(8) Å) to give a μ^3-oxygen bridged teflate group. The core of the structure is a distorted six-membered $(HgO_\mu)_3$ ring in which the Hg atoms are linked to one another through μ-oxygen bridged teflate groups. In addition, a μ^3-oxygen bridged teflate group caps each face of the $(HgO_\mu)_3$ ring. The μ^3-coordination descriptions for $O_{(1)}$ and $O_{(2)}$ are supported by the $O_{(1)}-Hg$ and $O_{(2)}-Hg$ bond orders (see Computational Results and Tables S6 and S7). The Hg and O_μ atoms of the $(HgO_\mu)_3$ ring are almost coplanar, with the ring atoms lying between 0.145 Å above and 0.191 Å below the average $(HgO_\mu)_3$ plane. The $Hg-O_\mu-Hg$ ring angles (95.1(4)−107.0(4)°) are similar to those of $[Hg(OTeF_5)_2\cdot 2N{\equiv}SF_3]_2$ (100.8(3)°), whereas the $O_\mu-Hg-O_\mu$ angles (136.3(4)−139.4(4)°) are significantly more open than those of $[Hg(OTeF_5)_2\cdot 2N{\equiv}SF_3]_2$ (79.2(3)°) to accommodate the larger ring size. The capping $Hg-O_\mu{}^3-Hg$ angles (84.2(3)−96.2(4)°) are smaller than the $Hg-O_\mu-Hg$ ring angles, and their $Hg-O_\mu{}^3$ bond lengths, $Hg-O_{(1)}$ (2.327(8), 2.501(8), 2.644(7) Å) and $Hg-O_{(2)}$ (2.143(7), 2.723(11), 2.781(11) Å), are significantly less than the sum of the F and Hg van der Waals radii (3.02 Å).[45,49] Although asymmetric, this appears to represent the first example of a μ^3-oxygen bridged F_5TeO- group. In addition, each $Hg_{(1)}$ and $Hg_{(3)}$ atom is

DOI: 10.1021/acs.inorgchem.5b01769
Inorg. Chem. 2015, 54, 9989−10000

Table 6. Selected Experimental Geometrical Parameters for $[Hg_3(OTeF_5)_5(N{=}SOF_2)\cdot 2N{\equiv}SF_3]_2$[a]

		Bond Lengths (Å)	
Hg_1-O_1	2.053(6)	Hg_3-N_1	2.185(8)
$Hg_1\cdots O_{1A}$	2.658(7)	Hg_3-N_2	2.340(12)
Hg_1-O_2	2.462(7)	Hg_3-N_3	2.284(8)
$Hg_1\cdots O_3$	2.711(7)	Hg_1-N_1	2.065(7)
Hg_2-O_3	2.077(6)	Hg_3-O_5	2.126(7)
Hg_2-O_4	2.027(8)		
Hg_2-O_2	2.506(7)	Te−O	1.806(8)−1.840(7)
Hg_2-O_5	2.501(7)	Te−F	1.800(8)−1.867(8)
	F_2OSN- group		NSF_3
N_1-S_1	1.483(8)	N−S	1.399(8)
S_1-O_6	1.415(8)	S−F	1.495(7)−1.509(7)
S−F	1.516(8), 1.526(8)		
		Bond Angles (deg)	
$Hg_1-O_2-Hg_2$	104.7(3)	$O_1-Hg_1-O_2$	92.2(3)
$Hg_2-O_5-Hg_3$	109.8(3)	$O_3-Hg_2-O_4$	169.3(3)
$Hg_3-N_1-Hg_1$	112.5(3)	$O_2-Hg_2-O_5$	72.7(3)
$N_1-Hg_1-O_2$	89.6(3)	$O_5-Hg_2-O_2$	69.1(3)
$N_1-Hg_1-O_1$	176.9(3)	$O_5-Hg_3-N_1$	132.1(3)
$O_1-Hg_1-O_{1A}$	75.2(3)	$Hg_1-O_1\cdots Hg_{1A}$	104.8(3)
$Hg_2-N_3-S_3$	152.0(6)	$Hg_1-N_1-S_1$	119.8(5)
$Hg_2-N_2-S_2$	155(1)	$Hg_3-N_1-S_1$	127.2(4)
	F_2OSN- group		NSF_3
N−S−O	122.9(4)	N−S−F	118.9(6)−123.4(7)
N−S−F	108.6(4), 109.0(5)	F−S−F	92.6(6)−98.1(6)
O−S−F	109.0(5), 109.1(4)		
F−S−F	94.3(5)		
		Dihedral Angle (deg)	
	$Te_4-O_4-Hg_2-O_3-Te_3$		40.7(6)

[a]The atom labeling scheme corresponds to that used in Figures 5 and S1. See Table S5 for a complete list of geometrical parameters.

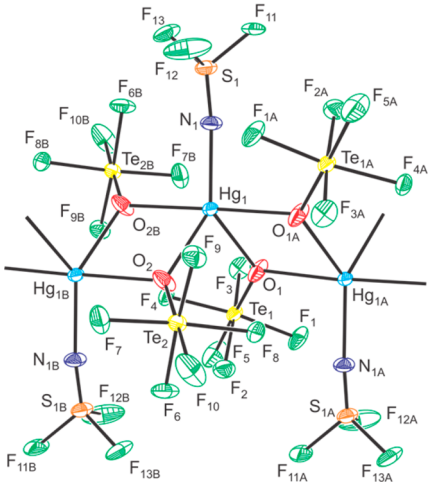

Figure 1. X-ray crystal structure of $[Hg(OTeF_5)_2\cdot N{\equiv}SF_3]_\infty$ showing the bonding to symmetry equivalent atoms in the chain structure and the orientations of the coordinated NSF_3 molecules along the *a*-axis of the unit cell. Thermal ellipsoids are shown at the 50% probability level.

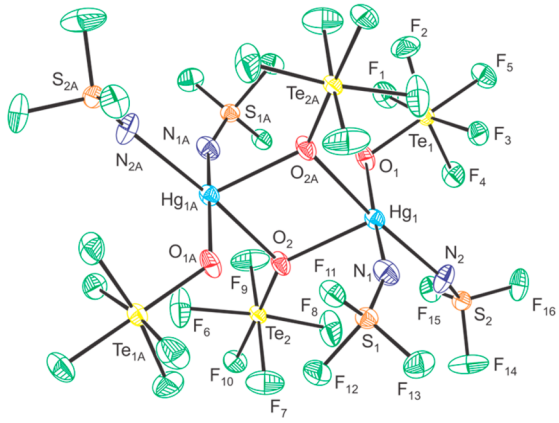

Figure 2. X-ray crystal structure of dimeric $[Hg(OTeF_5)_2\cdot 2N{\equiv}SF_3]_2$ showing the $(HgO_\mu)_2$ ring. Thermal ellipsoids are shown at the 50% probability level.

coordinated to two NSF_3 molecules, which are positioned above and below the $(HgO_\mu)_3$ ring, whereas the $Hg_{(2)}$ atom is coordinated to one terminal F_5TeO- group. The $Hg_{(2)}-O_{(6)}$ bond length of the terminal F_5TeO- group (2.051(9) Å) is comparable to those of $Hg(OTeF_5)_2$ (2.016(6) Å),[34] whereas the $Hg_{(2)}-O_{(2)}$ bond length is significantly elongated (2.143(7) Å). The $O_{(2)}-Hg_{(2)}-O_{(6)}$ bond angle (166.3(5)°) is close to that of free $Hg(OTeF_5)_2$ (170.5(4)°); however, the F_5TeO- groups adapt an essentially *syn*-conformation (dihedral $Te_{(2)}-O_{(2)}-Hg_{(2)}-O_{(6)}-Te_{(6)}$ angle, 5.8(8)°), contrasting with the *gauche*-conformation of the uncoordinated molecule (dihedral Te−O−Hg−O−Te angle, 53.7(3)°).[34] The asymmetric $Hg_{(2)}(OTeF_5)_2$ moiety results from the additional short $Hg_{(2)}-O_{(1)}$ contact (2.501(8) Å) and longer contacts with $O_{(2)}$ ($O_{(2)}\cdots Hg_{(1)}$, 2.781(11) Å; $O_{(2)}\cdots Hg_{(3)}$, 2.723(11) Å). The Hg−N bond lengths (2.223(10)−2.265(11) Å) are intermediate with respect to those of $[Hg(OTeF_5)_2\cdot 2N{\equiv}SF_3]_2$ (2.164(10), 2.377(10) Å). The geometrical parameters of the coordinated NSF_3 molecules (Table 4) are comparable to

DOI: 10.1021/acs.inorgchem.5b01769
Inorg. Chem. 2015, 54, 9989−10000

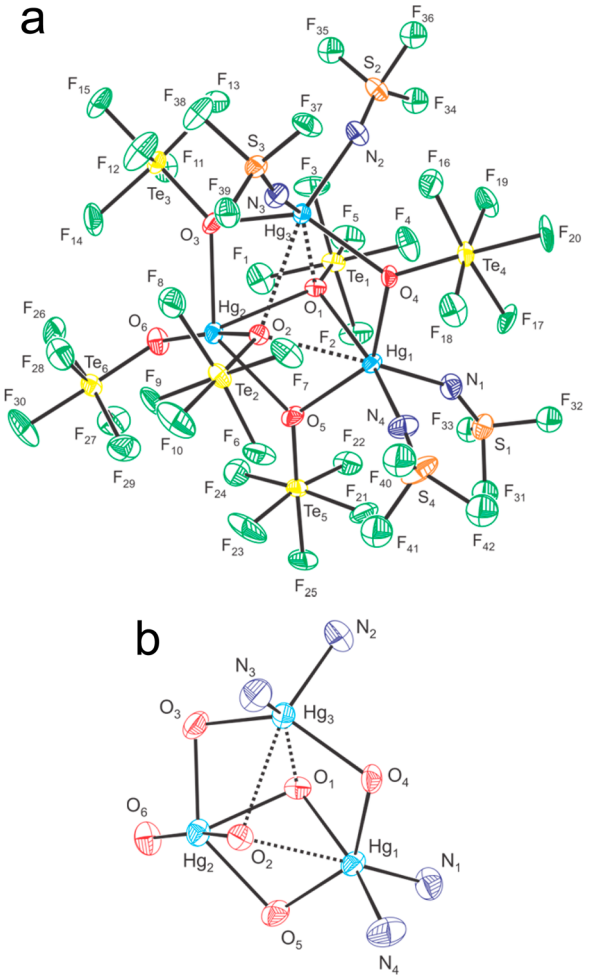

Figure 3. (a) The X-ray crystal structure of $[Hg_3(OTeF_5)_6{\cdot}4N{\equiv}SF_3]$ showing the $(HgO_\mu)_3$ ring and its capping F_5TeO- groups and (b) the coordination environments around the mercury atoms, where dashed lines indicate the longest bonding interactions. Thermal ellipsoids are shown at the (a) 30% probability level for greater clarity and (b) 50% probability level.

those of $[Hg(OTeF_5)_2{\cdot}2N{\equiv}SF_3]_2$ (see above) and do not require further commentary.

(d) $[Hg(OTeF_5)(N{=}SOF_2){\cdot}N{\equiv}SF_3]_\infty$. The crystal structure of $[Hg(OTeF_5)(N{=}SOF_2){\cdot}N{\equiv}SF_3]_\infty$ (Figure 4) consists of well-isolated chains which run along the *a*-axis of the crystallographic unit cell, with the shortest F---F (2.707(3)−2.935(3) Å) and F---O (2.841(3)−2.921(3) Å) distances being near the sum of the F and O van der Waals radii, 2.99 Å.[45] The infinite chains are comprised of three crystallographically unique Hg atoms which are bonded to bridging F_2OSN- and F_5TeO- groups. Each Hg atom is also coordinated to an NSF_3 molecule.

The coordination spheres of the Hg atoms are similar to that of $[Hg(OTeF_5)_2{\cdot}N{\equiv}SF_3]_\infty$, except a F_5TeO- ligand has been replaced by a N-bridged F_2OSN- ligand. Each Hg coordination sphere consists of two Hg−N bonds (2.109(2)−2.156(2) Å) with bridging F_2OSN- ligands, two longer Hg−O bonds (2.408(2)−2.537(2) Å) with bridging F_5TeO- ligands, and one longer Hg−N bond (2.496(3)−2.573(3) Å) with NSF_3. The Hg−N bridge bonds are much shorter than those of $[Hg(N_3)_3]^-$ (2.452(2), 2.485(4) Å),[48] whereas the Hg−N terminal bonds are much longer than the Hg−N terminal

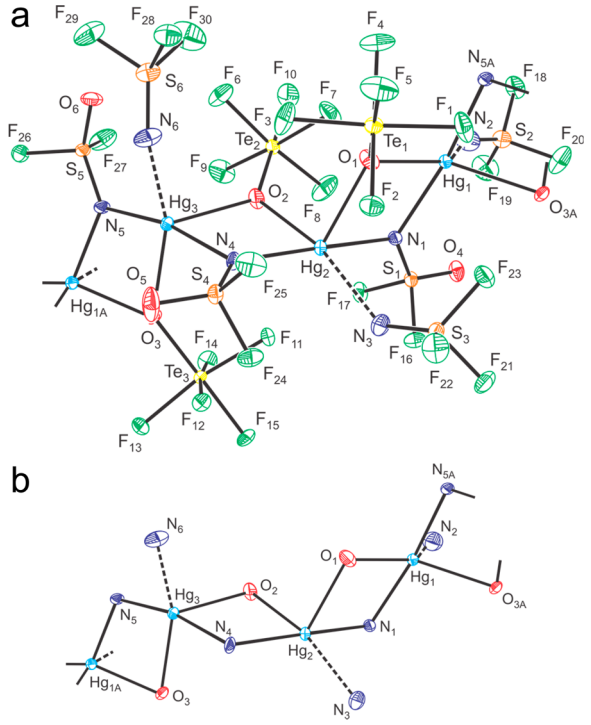

Figure 4. (a) The X-ray crystal structure of $[Hg(OTeF_5)(N{=}SOF_2){\cdot}N{\equiv}SF_3]_\infty$ showing (a) the repetitive unit of the chain and (b) the coordination environments of the mercury atoms. The dashed lines indicate the longest bonding interactions; thermal ellipsoids are shown at the 50% probability level.

bonds of the aforementioned adducts and $Hg(NSF_2)_2$ (2.050(13) Å).[47]

The NSF_3 molecules are more weakly coordinated than those of $[Hg(OTeF_5)_2{\cdot}N{\equiv}SF_3]_\infty$ (see above); consequently, the N−S (1.399(3)−1.407(3) Å) and S−F (1.520(2)−1.533(2) Å) bond lengths are equal, within $\pm 3\sigma$, to those of free NSF_3 (1.400(3) and 1.531(1)−1.534(2) Å, respectively).[10] The F_2OSN- ligands are readily distinguished from coordinated NSF_3 molecules by their substantially shorter S−O bonds (1.403(3)−1.407(2) Å) when compared with their S−F bonds (1.525(2)−1.540(2) Å). Furthermore, the N−S bonds (1.484(2)−1.488(3) Å) are significantly longer than the N≡S bond of NSF_3 (see above), indicative of the N═S character of the imido group. The bond lengths of the F_2OSN- groups are in good agreement with those of $[Mn(CO)_4NSOF_2]_2$ (N−S, 1.434(6) Å; S−O, 1.402(8) Å; S−F, 1.535(6), 1.556(6) Å),[29,30] and $[Ni(SO_2)_2][AsF_4(NSOF_2)_2]_2$ (N−S, 1.477(3), 1.476(4) Å; S−O, 1.389(3), 1.420(3)Å; S−F, 1.509(4)−1.528(5) Å).[31] The F_2OSN- ligands are also distinguishable by their bond angles. The Hg−N−S angles involving the F_2OSN- groups are significantly more closed (124.4(1)−124.5(1)°) than those associated with the terminal NSF_3 groups (141.5(2)−152.8(2)°). The coordination environments of the bridging N atoms are essentially planar, showing that the nitrogen atoms do not possess stereochemically active lone pairs and that they are formally sp^2-hybridized. Planar F_2OSN- groups have also been observed in $[Mn(CO)_4NSOF_2]_2$.[29,30]

(e) $[Hg_3(OTeF_5)_5(N{=}SOF_2){\cdot}2N{\equiv}SF_3]_2$. The structure (Figures 5 and S1) is related to that of $Hg_3(OTeF_5)_6{\cdot}4N{\equiv}SF_3$, with structural differences arising from the replacement of a μ-oxygen bridged $F_5TeO_{(2,4)}$ group by a μ-nitrogen bridged

DOI: 10.1021/acs.inorgchem.5b01769
Inorg. Chem. 2015, 54, 9989−10000

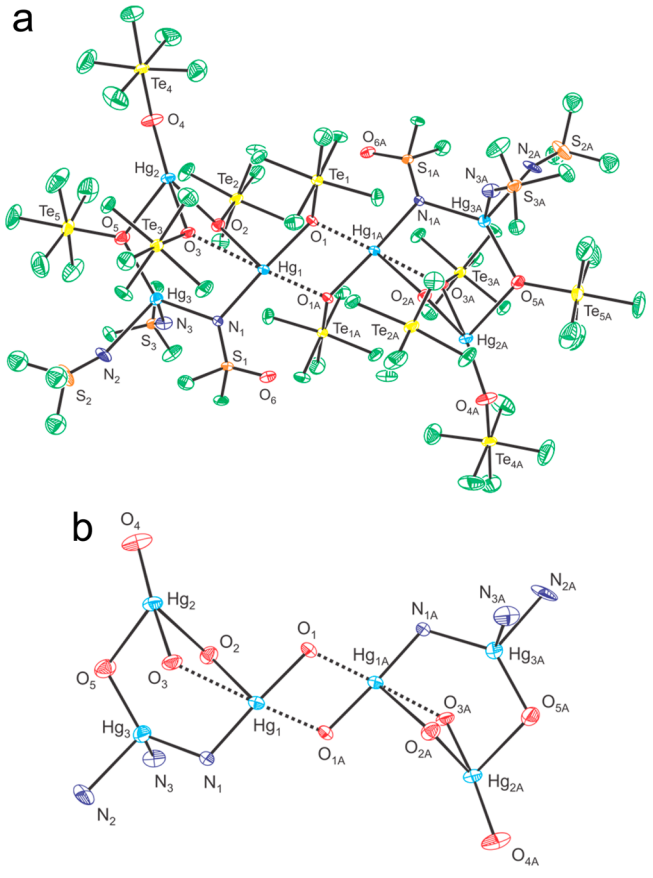

Figure 5. (a) The X-ray crystal structure of dimeric $[Hg_3(OTeF_5)_5(N{=}SOF_2)\cdot 2N{\equiv}SF_3]_2$ where the F atoms (green) are not labeled for clarity (see Figure S1 for the fully labeled structure) and (b) the coordination environments of mercury. The dashed lines indicate the longest bonding interactions. Thermal ellipsoids are shown at the (a) 30% probability level for clarity and (b) 50% probability level.

F_2OSN- group. Furthermore, $Hg_{(1)}$ is no longer coordinated to two NSF_3 molecules; instead, two asymmetric $Hg_3(OTeF_5)_5(N{=}SOF_2)\cdot 2N{\equiv}SF_3$ units interact through $Hg_{(1)}{\cdots}O_{\mu(1A)}$ and $Hg_{(1A)}{\cdots}O_{\mu(1)}$ contacts ($2 \times 2.658(7)$ Å) to form a dimer. The dimers are well-isolated from one another in their crystal lattice, with the shortest F···F intermolecular contacts ranging from 2.676(10) to 2.937(11) Å. The structure of the asymmetric unit may be formally described as the interaction of a $Hg_{(2)}(OTeF_5)_2$ molecule with a $Hg_2(OTeF_5)_3(NSOF_2)(N{\equiv}SF_3)_2$ moiety to form a distorted (Hg_3O_2N) ring.

The $Hg_{(2)}(OTeF_5)_2$ unit (dihedral Te−O−$Hg_{(2)}$−O−Te angle, 40.7(6)°) retains the *gauche*-conformation observed in the crystal structure of $Hg(OTeF_5)_2$ (∠Te−O−Hg−O−Te, 53.7(3)°) and, correspondingly, the $Hg_{(2)}$−O bond lengths ($O_{(4)}$, 2.027(8); $O_{(3)}$, 2.077(6) Å) and $O_{(3)}$−$Hg_{(2)}$−$O_{(4)}$ bond angle (169.3(2)°) are comparable to those of $Hg(OTeF_5)_2$ (2.016(6) Å; 170.5(4)°).[34] The $Hg_{(2)}(OTeF_5)_2$ unit also interacts with two bridging F_5TeO- groups ($Hg_{(2)}$−O, 2.506(7), 2.501(7) Å). The $Hg_{(3)}$ atom is coordinated to two NSF_3 molecules ($Hg_{(3)}$−N, 2.260(8), 2.284(8) Å), one bridging F_5TeO- group ($Hg_{(3)}$−$O_{(5)}$, 2.126(7) Å), and a bridging F_2OSN- group ($Hg_{(3)}$−$N_{(1)}$, 2.185(8) Å). The $Hg_{(1)}$ coordination environment consists of a bridging F_5TeO- group ($Hg_{(1)}$−$O_{(2)}$, 2.462(7) Å), a bridging F_2OSN- group ($Hg_{(1)}$−$N_{(1)}$, 2.065(5) Å), and a terminal $F_5TeO_{(1)}$ group ($Hg_{(1)}$−$O_{(1)}$, 2.053(6) Å). In addition, $Hg_{(1)}$ and $Hg_{(1A)}$ have long contacts with $O_{(1A)}$ and $O_{(1)}$, respectively, of the symmetry-related $F_5TeO_{(1,1A)}$ groups (Figure 5). These contacts result in dimer formation and a $(HgO)_2$ ring as found in $[Hg(OTeF_5)_2\cdot 2N{\equiv}SF_3]_2$. The structural parameters of the coordinated NSF_3 molecules and F_2OSN- ligand, including the Hg−N bond lengths and Hg−N−S bond angles, are similar to those of $[Hg(OTeF_5)(NSOF_2)\cdot N{\equiv}SF_3]_\infty$ and do not require further commentary.

Raman Spectroscopy. The Raman spectra of $[Hg(OTeF_5)_2\cdot 2N{\equiv}SF_3]_2$ (**2**), $Hg_3(OTeF_5)_6\cdot 4N{\equiv}SF_3$ (**3**), $[Hg(OTeF_5)(N{=}SOF_2)\cdot N{\equiv}SF_3]_\infty$ (**4**), and $[Hg_3(OTeF_5)_5(N{=}SOF_2)\cdot 2N{\equiv}SF_3]_2$ (**5**) were recorded at −150 °C (Figures S2–S5 and Table S8). The spectra are complex due to the presence of several crystallographically distinct F_5TeO- groups, whose Raman bands overlap with those of NSF_3 and the F_2OSN- group, preventing their unambiguous assignments. However, a significant number of nonoverlapping bands could be assigned by comparison with the literature.

Raman bands centered at approximately 1190 cm^{-1} ((**4**), 1191, 1196 cm^{-1}; (**5**), 1187, 1199 cm^{-1}) were assigned to S−N stretching modes of F_2OSN- ligands by comparison with those reported for $Hg(NSOF_2)_2$ (1191 cm^{-1}),[21] $(CH_3)_3SiNSOF_2$ (1191 cm^{-1}),[21] $[Hg(NSOF_2)_4]^{2-}$ (1180 cm^{-1}),[33] $[Ni(SO_2)_2][AsF_4(NSOF_2)_2]_2$ (1190 cm^{-1}),[31] and $Cu(NSOF_2)(AsF_5NSOF_2)$ (1173, 1198 cm^{-1}).[31] A weak band at 1391 cm^{-1} (**4**) was assigned to $\nu_{as}(SO)$ of the F_2OSN- ligand by comparison with $Hg(NSOF_2)_2$ (1396 cm^{-1}), $(CH_3)_3SiNSOF_2$ (1365, 1396 cm^{-1}), $[Ni(SO_2)_2][AsF_4(NSOF_2)_2]_2$ (1409 cm^{-1}), and $Cu(NSOF_2)(AsF_5NSOF_2)$ (1398, 1410 cm^{-1}). It is noteworthy that the Raman spectra of **2** and **3** are devoid of vibrational bands within this frequency range, in accordance with the observation that the F_2OSN- derivatives, **4** and **5**, do not form at significant rates at 0 °C (see Syntheses).

Bands in the 1514−1622 cm^{-1} region of the spectrum were assigned to $\nu(SN)$ of coordinated NSF_3 by comparison with those of $[F_3S{\equiv}NXeF]^+$ (1527−1548 cm^{-1}),[15] $[Mn(N{\equiv}SF_3)_4][AsF_6]_2$ (1580 cm^{-1}),[16] $F_5AsN{\equiv}SF_3$ (1610 cm^{-1}),[3] and $[Re(CO)_5N{\equiv}SF_3][AsF_6]$ (1643 cm^{-1}).[20] Overall, S−N stretching bands are shifted to higher frequency relative to those of free NSF_3 (1503−1524 cm^{-1}).[8] The lowest frequency bands (1514−1545 cm^{-1}) observed for **4** correlate with the weakest Hg−NSF_3 bonds (Hg−N, 2.496(3)−2.573(3) Å), whereas the highest frequency bands (1553−1622 cm^{-1}) were observed for **2** and correlate with the shortest Hg−NSF_3 bonds (2.164(10) Å). The remaining $\nu(SN)$ frequencies and Hg−N bond lengths fall between the aforementioned extremes. In this instance, X-ray crystallography fails to reliably differentiate among S−N bond lengths, whereas the S−N stretching frequencies clearly show increases upon adduct formation.

In contrast with the S−N bond lengths, the S−F bond lengths are more sensitive to donor−acceptor interactions, displaying shorter S−F bonds upon NSF_3 coordination. Correspondingly, the S−F stretching frequencies shift to higher frequencies, as observed for $[F_3S{\equiv}NXeF]^+$ (869−952 cm^{-1}).[15] The bands between 844 and 909 cm^{-1} in the Raman spectra of **2** and **3** can be confidently assigned to $\nu_{as}(SF_3)$ stretches by comparison with those of $[Mn(CO)_5N{\equiv}SF_3][AsF_6]$ (882 cm^{-1}), $[CpFe(CO)_2N{\equiv}SF_3][AsF_6]$ (876, 888 cm^{-1}), and $[Re(CO)_5N{\equiv}SF_3][AsF_6]$ (889, 900 cm^{-1}).[20] In the cases of **4** and **5**, the $\nu_{as}(SF_2)$ bands of their F_2OSN- groups overlap with this region of the spectrum. For comparison, the $\nu_{as}(SF_2)$ bands of $(CH_3)_3SiNSOF_2$[21] occur at 810 and 853 cm^{-1}. The spectral region between 748 and 838 cm^{-1} in **2**−**5** is associated with the

DOI: 10.1021/acs.inorgchem.5b01769
Inorg. Chem. 2015, 54, 9989−10000

symmetric counterparts, $\nu_s(SF_3)$ and $\nu_s(SF_2)$, but is also complicated by overlap with $[\nu(Hg{-}O) - \nu(Te{-}O)]$-type stretching modes. The most intense band is found in this range and is assigned to $\nu_s(SF_3)$ ((**2**) 833, (**3**) 819, (**4**) 808, and (**5**) 821 cm^{-1}). The bands lying between 603 and 719 cm^{-1} are characteristic of $\nu(Te{-}F_{eq})$ and $\nu(Te{-}F_{ax})$ stretching modes and are comparable to those of $Hg(OTeF_5)_2$ (624−735 cm^{-1}),[34] $Hg(OTeF_5)_2{\cdot}1.5XeF_2$ (623−753 cm^{-1}),[34] and $[Hg_2(OTeF_5)_6]^{2-}$ (604−707 cm^{-1}).[35] Bands appearing between 472 and 514 cm^{-1} are assigned to $[\nu(Hg{-}O) + \nu(Te{-}O)]$-type stretching modes by comparison with $Hg(OTeF_5)_2$ (472−511 cm^{-1}) and its derivatives.[34,35]

The bands lying between 541 and 579 cm^{-1} in the Raman spectra of **2** and **3** are assigned to $\delta_s(SF_3)_{NSF_3}$ by comparison with NSF_3 (526 and 530 cm^{-1})[8] and $[F_3S{\equiv}NXeF]^+$ (556−570 cm^{-1}).[15] The bands between 535 and 575 cm^{-1} in the spectra of **4** and **5** may also be assigned to $\delta_s(NSF_2)_{NSOF_2}$ as observed in $[Hg(NSOF_2)_4]^{2-}$ (555 cm^{-1}).[33] Bands at 436−450 and 331−412 cm^{-1} in the spectra of **2** and **3** are assigned to $\delta_s(NSF_2)_{NSF_3}$ and $\delta_{as}(NSF_2)_{NSF_3}$, respectively, by comparison with those of NSF_3 (438, 445; 349, 355 cm^{-1})[8] and $[F_3S{\equiv}NXeF]^+$ (448, 471; 357, 369 cm^{-1}).[15]

Computational Results. Quantum-chemical calculations were carried out to gain insight into the bonding of the μ^3-oxygen bridged teflate groups observed in structure (**3**) (see X-ray Crystallography). The electronic structure of $Hg_3(OTeF_5)_6{\cdot}4N{\equiv}SF_3$ (C_1) was optimized, with all frequencies real, at the PBE1PBE/def2-SVP level of theory (Table S6 and Figure 6).

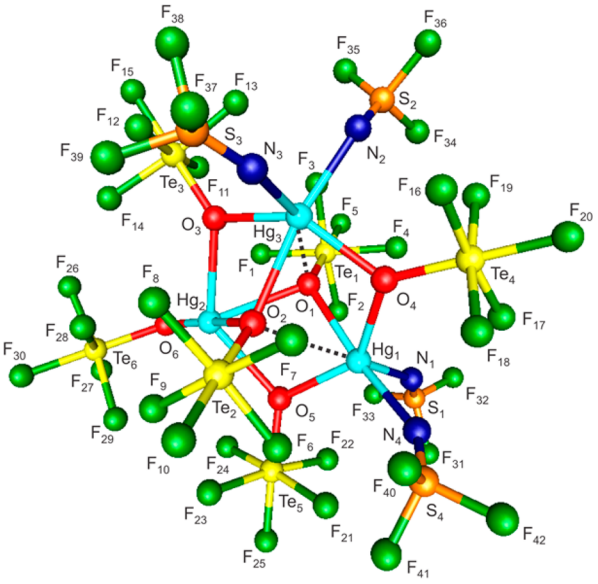

Figure 6. Gas-phase, energy-minimized geometry of $Hg_3(OTeF_5)_6{\cdot}4N{\equiv}SF_3$ (C_1) calculated at the PBE1PBE/def2-SVP level of theory. The longest bonding interactions are denoted by dashed lines.

The experimental geometry is well reproduced by the calculations, in particular its bicapped $(HgO_\mu)_3$ ring and capping F_5TeO- groups. The Hg−N bond lengths are all overestimated by 0.08−0.10 Å. All Hg−O bond lengths are well reproduced except $Hg_3{-}O_2$, which is underestimated by 0.21 Å. The calculated geometry reproduces the three types of $Hg{-}O_{(TeF_5)}$ bonds encountered in the experimental structure of **3**, i.e., those involving terminal F_5TeO- groups and μ- and μ^3-O bridging F_5TeO- groups. As observed in the experimental structure, the μ^3-O atoms are asymmetrically coordinated to the mercury centers. Although the valences and charges remain nearly constant for all oxygen atoms, ranging from 0.80 to 0.85 and −1.11 to −1.22, respectively, the bond orders vary significantly and correlate with their experimental and calculated Hg−O bond lengths. The Hg−O bond order is greatest for the terminal F_5TeO- group (O_6, 0.24) and decreases significantly for the μ-O bridged F_5TeO- groups (O_3, 0.08 and 0.13; O_4, 0.10 and 0.11; O_5, 0.07 and 0.13) and the μ^3-O bridged F_5TeO- groups (O_1, 0.06, 0.07 and 0.10; O_2, 0.04, 0.07 and 0.15). It is noteworthy that the $Hg{-}O_\mu{}^3$ bond orders are comparable to the $Hg{-}O_\mu$ bond orders. The calculated Te−O bond lengths do not vary significantly, nor do the Te−O bond orders (Table S7).

CONCLUSION

Donor−acceptor adducts form between the Lewis acidic Hg(II) center of $Hg(OTeF_5)_2$ and the nitrogen base, NSF_3, at 0 °C, yielding $[Hg(OTeF_5)_2{\cdot}N{\equiv}SF_3]_\infty$ (**1**), $[Hg(OTeF_5)_2{\cdot}2N{\equiv}SF_3]_2$ (**2**), and $Hg_3(OTeF_5)_6{\cdot}4N{\equiv}SF_3$ (**3**). When these reactions are carried out at room temperature, nucleophilc attack by a F_5TeO- group at the sulfur(VI) atom of NSF_3 occurs, followed by O/F metathesis between Hg-coordinated NSF_3 molecules and F_5TeO- ligands, and TeF_6 elimination to give the structurally related F_2OSN- derivatives, $[Hg(OTeF_5){-}(N{=}SOF_2){\cdot}N{\equiv}SF_3]_\infty$ (**4**) and $[Hg_3(OTeF_5)_5(N{=}SOF_2){\cdot}2N{\equiv}SF_3]_2$ (**5**). The Raman bands associated with the coordinated NSF_3 molecules and F_2OSN- ligands were tentatively assigned for compounds **2**−**5** by comparison with other NSF_3 adducts and F_2OSN- derivatives, confirming that the F_2OSN- group is only formed at a significant rate above 0 °C. These compounds exhibit a variety of structural motifs, including the infinite chain structures of **1** and **4**; a dimeric structure, **2**, based on a $(HgO_\mu)_2$ ring at its core; **3**, a cage structure comprised of an $(HgO_\mu)_3$ ring that is capped on either side by two μ^3-oxygen bridged F_5TeO- groups; and **5**, a dimeric structure that possesses two distorted (Hg_3O_2N) rings. The description of the capping F_5TeO- groups of (**3**) as μ^3-oxygen bridged is supported by the calculated gas-phase geometry and Mayer bond orders. Teflate groups that form μ^2-oxygen bridges between mercury centers are encountered in all five structures, a recurrent structural feature in group 11 and 12 metal teflate species.[35−42] Compounds **1**−**5** represent a novel class of neutral transition metal complexes with NSF_3, providing the first examples of NSF_3 coordination to mercury. Compounds **4** and **5** also provide the only examples of F_2OSN- derivatives of mercury that have been characterized by single-crystal X-ray diffraction.

EXPERIMENTAL SECTION

Apparatus and Materials. *(a) General.* Manipulations involving air-sensitive materials were carried out under anhydrous conditions on glass and metal high-vacuum lines and inside an inert atmosphere drybox as previously described.[50] Preparative work was carried out in T-shaped reaction vessels constructed from 1/4-in. o.d. lengths (1/32-in. wall thickness) of FEP (tetrafluoroethylene-hexafluoropropylene block copolymer) tubing.[50] The tubing was heat-sealed at one end, heat flared at the other end, and connected through a 45° SAE flare nut to the conical end of a Kel-F (chlorotrifluoroethylene polymer) valve to form a compression seal. Reaction vessels and sample tubes were rigorously dried under dynamic vacuum for at least 8 h prior to passivation with 1 atm of F_2 gas. Vacuum line connections were made

DOI: 10.1021/acs.inorgchem.5b01769
Inorg. Chem. 2015, 54, 9989−10000

using 1/4-in. 316 stainless steel Swagelok Ultratorr unions fitted with Viton O-rings.

Literature methods were used to prepare $Hg(OTeF_5)_2$[34] and NSF_3[51] in high purity and to purify SO_2ClF (Allied Chemical, Baker Adamson Division).[52] Liquid SO_2 (Aldrich) and Freon-114 (1,2-dichlorotetrafluoroethane, Aldrich) were dried over P_2O_5 prior to use. Nitrogen gas (99.995%, H_2O < 0.5 ppm, Praxair) was used for backfilling reaction and sample vessels.

(b) Syntheses and Crystal Growth. In a drybox, $Hg(OTeF_5)_2$ was weighed into an FEP reaction vessel at room temperature. The vessel was transferred to a metal vacuum line where it was connected to an FEP vessel (−78 °C) containing NSF_3. All connections were dried under dynamic vacuum and thoroughly passivated with F_2. The NSF_3 storage vessel was warmed to 0 °C prior to condensing NSF_3 into the reaction vessel at −78 °C. Sufficient NSF_3 was used to cover the solid $Hg(OTeF_5)_2$ with liquid NSF_3 when the reaction mixture was warmed to −50 °C. The appropriate solvent was then condensed onto the frozen reaction mixture at −78 °C and warmed to either 0 °C or to room temperature to effect dissolution and reaction. Crystals suitable for X-ray structure determinations were grown by cooling the side arm of the reaction vessel to −78 °C to establish a thermal gradient for the slow distillation of the solvent from the reaction mixture into the side arm of the reaction vessel. The side arm containing the condensed solvent was then cooled to −196 °C and heat-sealed off under dynamic vacuum. Low-temperature Raman spectra (−150 °C) were recorded on the crystalline sample.

(i) $[Hg(OTeF_5)_2{\cdot}N{\equiv}SF_3]_\infty$. The reagents, $Hg(OTeF_5)_2$ (0.0937 g, 0.1382 mmol) and excess NSF_3, were combined in an FEP reaction vessel followed by condensation of ∼0.5 mL of SO_2ClF at −78 °C and backfilled with 400 Torr of dry N_2. The solution was then warmed to 0 °C, and a thermal gradient was established for crystal growth by cooling the reactor side arm to −78 °C. Colorless needles grew over a period of ca. 2 days. A crystal having the dimensions 0.03 × 0.03 × 0.22 mm^3 was selected for a low-temperature X-ray crystal structure determination. Unit cell determinations on several crystals and Raman spectroscopy established that $[Hg(OTeF_5)_2{\cdot}N{\equiv}SF_3]_\infty$ was a minor product and that the bulk sample was mostly comprised of $[Hg(OTeF_5)_2{\cdot}2N{\equiv}SF_3]_2$.

(ii) $[Hg(OTeF_5)_2{\cdot}2N{\equiv}SF_3]_2$. The reagents, $Hg(OTeF_5)_2$ (0.1139 g, 0.1681 mmol) and excess $N{\equiv}SF_3$, were combined in an FEP reaction vessel. Freon-114 (∼0.4 mL) was condensed onto the reaction mixture at −78 °C and the reactor was backfilled to 400 Torr with dry N_2 before warming to 0 °C to dissolve the reactants. Colorless, plate-shaped crystals were grown by slow solvent evaporation over a 5 h period by cooling the side arm to −78 °C. A crystal having the dimensions 0.05 × 0.11 × 0.13 mm^3 was selected for a low-temperature X-ray structure determination.

(iii) $Hg_3(OTeF_5)_6{\cdot}4N{\equiv}SF_3$. The reactants, $Hg(OTeF_5)_2$ (0.1298 g, 0.1914 mmol) and excess NSF_3, were combined in an FEP reaction vessel with ∼0.3 mL of Freon-114 solvent and the reactor was backfilled to 400 Torr with dry N_2. Crystals were grown over a 12 h period by cooling the side arm of the reactor to −78 °C. Colorless needles remained after all of the solvent had transferred. A crystal having the dimensions 0.04 × 0.07 × 0.26 mm^3 was selected for a low-temperature X-ray structure determination. The crystalline sample was primarily composed of $[Hg(OTeF_5)_2{\cdot}2N{\equiv}SF_3]_2$, which was identified by unit cell determinations on several crystals and by Raman spectroscopy. A second reaction was carried out under similar conditions using 0.0718 g (0.1059 mmol) of $Hg(OTeF_5)_2$ in SO_2ClF solvent at room temperature (under 400 Torr N_2). This sample rapidly crystallized over a 3 h period and only resulted in $Hg_3(OTeF_5)_6{\cdot}4N{\equiv}SF_3$, which was identified by unit cell determinations on several crystals and by the Raman spectrum of the bulk sample. No vibrational bands attributable to the F_2OSN- group were observed.

(iv) $[Hg(OTeF_5)(N{=}SOF_2){\cdot}N{\equiv}SF_3]_\infty$. A reaction vessel was loaded with $Hg(OTeF_5)_2$ (0.0905 g, 0.1335 mmol), and excess NSF_3 was condensed onto the solid at −78 °C followed by ∼0.3 mL of SO_2ClF solvent. The void above the solution was backfilled with 800 Torr of dry N_2 at −78 °C, and the mixture was warmed to room temperature to dissolve the reactants. The side arm was cooled to −78 °C in order to create a temperature gradient. Colorless needles formed after 3 days. The remaining solution was decanted into the side arm of the reaction vessel and removed by heat-sealing off the side arm and contents under dynamic vacuum at −196 °C. A crystal having the dimensions 0.05 × 0.05 × 0.56 mm^3 was selected for a low-temperature X-ray structure determination. The crystalline product was transferred into a dry 1/4-in. o.d. Pyrex glass tube, sealed using a Swagelok Ultratorr plug, and the Raman spectrum was recorded. The reaction was repeated in Freon-114 and was allowed to react at room temperature for 11 days. On the basis of the Raman spectrum and multiple unit cell determinations, only $[Hg(OTeF_5)(N{=}SOF_2){\cdot}N{\equiv}SF_3]_\infty$ had formed.

(v) $[Hg_3(OTeF_5)_5(N{=}SOF_2){\cdot}2N{\equiv}SF_3]_2$. The reagents, $Hg(OTeF_5)_2$ (0.1406 g, 0.2074 mmol) and excess NSF_3, were combined in an FEP reaction vessel, and SO_2 (∼0.3 mL) was condensed onto the reagents at −78 °C. The reactor and contents were backfilled to 800 Torr with dry N_2 at −78 °C and warmed to room temperature to dissolve the reactants. Crystals were grown at room temperature by solvent evaporation over a 12 h period by cooling the side arm of the vessel to −78 °C, resulting in colorless plates. A crystal having the dimensions 0.05 × 0.08 × 0.14 mm^3 was selected for a low-temperature X-ray structure determination.

X-ray Crystallography. *(a) Crystal Mounting Procedure.* All crystalline products were stored at −78 °C until a suitable crystal could be selected and mounted on an X-ray diffractometer using a previously described low-temperature crystal mounting procedure.[35,53]

(b) Collection and Reduction of X-ray Data. Single crystals were centered on a SMART APEX II diffractometer, equipped with an APEX II 4K charge-coupled device (CCD) and a triple-axis goniometer, controlled by the APEX2 Graphical User Interface (GUI) software.[54] A Bruker Triumph curved crystal monochromator and a Mo Kα (λ = 0.71073 Å) source were used. For all X-ray diffraction data sets, the ϕ-rotations and ω-scans were fixed at χ = 54.74° and collected at 0.5° intervals.

The $[Hg(OTeF_5)_2{\cdot}N{\equiv}SF_3]_\infty$ data set consisted of a quarter-sphere of ϕ-rotations (4629 frames) and a series of ω-rotations (738 frames) with an exposure time of 11 s. The data sets of $[Hg(OTeF_5)(N{=}SOF_2){\cdot}N{\equiv}SF_3]_\infty$ and $[Hg(OTeF_5)_2{\cdot}2N{\equiv}SF_3]_2$ each consisted of a half-sphere of ϕ-rotations (2020 frames) with exposure times of 20 and 25 s, respectively. The data sets of $Hg_3(OTeF_5)_6{\cdot}4N{\equiv}SF_3$ and $[Hg_3(OTeF_5)_5(N{=}SOF_2){\cdot}2N{\equiv}SF_3]_2$ (in square brackets) consisted of a full-sphere of ϕ-rotations (1616 [2832] frames) and an additional series of ω-rotations for $[Hg_3(OTeF_5)_5(N{=}SOF_2){\cdot}2N{\equiv}SF_3]_2$ (360 frames) using exposure times of 30 [20] s. All diffraction data were processed by use of the APEX2 GUI software,[54] which applied Lorentz and polarization corrections to the three-dimensionally integrated diffraction spots. The program SADABS[55] was used for scaling the diffraction data, the application of decay corrections, and empirical absorption corrections based on redundant reflections.

(c) Solution and Refinement of the Structures. The XPREP[56] program was used to confirm the crystal system and the space group. The structures were solved in their respective space groups by use of direct methods using SHELXS[56] or SIR92,[57] and the solutions yielded the positions of all the heavy atoms as well as some of the lighter atoms. Successive difference Fourier syntheses revealed the positions of the remaining light atoms. The final refinements were obtained by introducing anisotropic parameters for all the atoms, an extinction parameter, and the recommended weighting factor. The maximum electron densities in the final difference Fourier maps were located around the heavy atoms. The PLATON program[57] could not suggest additional or alternative symmetries.

Structure refinements of $[Hg(OTeF_5)_2{\cdot}2N{\equiv}SF_3]_2$ and $[Hg(OTeF_5)(N{=}SOF_2){\cdot}N{\equiv}SF_3]_\infty$ were straightforward. In the structure of $[Hg_3(OTeF_5)_5(N{=}SOF_2){\cdot}2N{\equiv}SF_3]_2$, one NSF_3 molecule was disordered among three equally populated orientations. Two NSF_3 molecules were twofold (50/50) disordered in the structure of $Hg_3(OTeF_5)_6{\cdot}4N{\equiv}SF_3$. The NSF_3 molecule of $[Hg(OTeF_5)_2{\cdot}N{\equiv}SF_3]_\infty$ was disordered among three equally populated orientations, and both terminal teflate groups were found to be twofold disordered (50/

DOI: 10.1021/acs.inorgchem.5b01769
Inorg. Chem. 2015, 54, 9989−10000

50). The disorders were dealt with by using the command SAME.[56] The disordered groups shared a common central sulfur or tellurium atom; as a consequence, the fluorine atoms of the disordered entities were refined isotropically.

^{19}F NMR Spectroscopy. *(a) Instrumentation.* Fluorine-19 NMR spectra were recorded unlocked (field drift <0.1 Hz h^{-1}) on a Bruker Avance-500 spectrometer equipped with an 11.744-T cryomagnet. The NMR probe was cooled using a nitrogen flow and variable temperature controller (BVT-3000). Fluorine-19 NMR spectra were acquired at −35 °C using a 5-mm broad band reverse probe operating at 470.631 MHz. Spectra were recorded in 65K memory, with a spectral width setting of 47 kHz, yielding data-point resolutions of 0.72 Hz/data point and acquisition times of 1.43 s. The pulse width, corresponding to a bulk magnetization tip angle of approximately 90°, was 10 μs. A relaxation delay of 2.00 s was used, and 128 transients were accumulated. A line broadening of 0.50 Hz was used in the exponential multiplication of the free induction decays prior to Fourier transformation. Fluorine-19 spectra were referenced externally at −35 °C to samples of neat $CFCl_3$. The chemical shift convention used is a positive (negative) sign indicates a chemical shift to high (low) frequency of the reference compound.

(b) Sample Preparation. A ^{19}F NMR sample was prepared to support the postulated reaction pathway given in Scheme 1. A T-shaped reaction vessel was constructed from a 1/4-in. o.d. length of FEP tubing that was fused to a 4-mm o.d. length of FEP tubing. The latter served as a side arm and NMR sample tube. To the 1/4-in. section of the reaction vessel, 0.1027 g (0.1515 mmol) of $Hg(OTeF_5)_2$ was added in a drybox followed by condensation of excess NSF_3 and ∼0.3 mL of Freon-114 solvent at −196 °C. The reaction vessel was warmed to −78 °C, backfilled to 400 Torr with dry N_2, and was allowed to react at room temperature, with periodic agitation, for 24 h. The 4-mm o.d. side arm/NMR tube was cooled to −78 °C to establish a thermal gradient for the distillation of volatiles from the reaction mixture. When distillation appeared to be complete, both arms of the reaction vessel were cooled to −196 °C, and N_2 was removed under a dynamic vacuum. The 1/4-in. section of the reaction vessel was warmed to room temperature under static vacuum to ensure all volatiles had condensed into the side arm/NMR tube immediately before it was heat-sealed at −196 °C under dynamic vacuum. The colorless solution was stored at −78 °C until the ^{19}F NMR spectrum could be recorded. The 4-mm FEP sample tube was inserted into a 5-mm o.d. thin wall precision glass NMR tube (Wilmad) prior to recording the ^{19}F NMR spectrum.

Raman Spectroscopy. Raman spectra were recorded on a Bruker RFS 100 FT-Raman spectrometer at −150 to −155 °C using 1064-nm excitation at a laser power of 500 mW, and 1 cm^{-1} resolution as previously described.[53] A total of 1000 scans were acquired for each spectrum. Raman spectra of the crystalline solids were recorded in 1/4-in. o.d. FEP reaction vessels, except for the spectrum of $[Hg(OTeF_5)(N{=}SOF_2){\cdot}N{\equiv}SF_3]_\infty$, which was recorded in a 1/4-in. o.d. Pyrex glass tube.

Computational Details. The optimized gas-phase geometry of $Hg_3(OTeF_5)_6{\cdot}4N{\equiv}SF_3$ was obtained at the PBE1PBE level of theory using the def2-SVP basis sets. The basis sets were obtained online from the EMSL Basis Set Exchange (https://bse.pnl.gov/bse/portal).[58] Quantum-chemical calculations were carried out using the program Gaussian 09[59] for geometry optimizations and vibrational frequencies and intensities. Natural bond orbital analyses were performed using the NBO program (version 6.0).[60]

■ ASSOCIATED CONTENT

Supporting Information

The Supporting Information is available free of charge on the ACS Publications website at DOI: 10.1021/acs.inorgchem.5b01769.

Experimental geometrical parameters for **1** (Table S1), **2** (Table S2), **3** (Table S3), **4** (Table S4), and **5** (Table S5), fully labeled X-ray crystal structure of dimeric $[Hg_3(OTeF_5)_5(N{=}SOF_2){\cdot}2N{\equiv}SF_3]_2$ (Figure S1), calculated geometrical parameters (Table S6) and NBO data for **3** (Table S7), experimental Raman frequencies for **2**−**5** (Table S8), Raman spectra for **2**−**5** (Figures S2−S5) (PDF)

X-ray crystallographic files for the structure determinations of **1**−**5** (CIF)

■ AUTHOR INFORMATION

Corresponding Author

*E-mail: schrobil@mcmaster.ca.

Notes

The authors declare no competing financial interest.

■ ACKNOWLEDGMENTS

We thank the Natural Sciences and Engineering Research Council of Canada for support in the form of a Discovery Grant (G.J.S.) and an Alexander Graham Bell Canada Graduate Scholarship (J.R.D.), and SHARCNet (Shared Hierarchical Academic Research Computing Network; www.sharcnet.ca) for providing the computational resources. We also thank J.P. Paxon for some of the preliminary synthetic work relating to $[Hg(OTeF_5)(N{=}SOF_2){\cdot}N{\equiv}SF_3]_\infty$.

■ REFERENCES

(1) Glemser, O.; Mews, R. *Adv. Inorg. Chem. Radiochem.* **1972**, *14*, 333−390.
(2) Mews, R. *Adv. Inorg. Chem. Radiochem.* **1976**, *19*, 185−237.
(3) Glemser, O.; Mews, R. *Angew. Chem., Int. Ed. Engl.* **1980**, *19*, 883−899.
(4) Roesky, H. W. *J. Fluorine Chem.* **1999**, *100*, 217−226.
(5) Richert, H.; Glemser, O. *Z. Anorg. Allg. Chem.* **1961**, *307*, 328−344.
(6) Glemser, O.; Richert, H. *Z. Anorg. Allg. Chem.* **1961**, *307*, 313−327.
(7) Königer, F.; Müller, A.; Glemser, O. *J. Mol. Struct.* **1978**, *46*, 29−34.
(8) Müller, A.; Ruoff, A.; Krebs, B.; Glemser, O.; Koch, W. *Spectrochim. Acta, Part A* **1969**, *25*, 199−205.
(9) Kirchhoff, W. H.; Wilson, E. B., Jr. *J. Am. Chem. Soc.* **1962**, *84*, 334−336.
(10) Borrmann, T.; Lork, E.; Mews, R.; Parsons, S.; Petersen, J.; Stohrer, W.-D.; Watson, P. G. *Inorg. Chim. Acta* **2008**, *361*, 479−486.
(11) Glemser, O.; Koch, W. *An. Asoc. Quim. Argent.* **1971**, *59*, 143−148.
(12) Müller, A.; Glemser, O.; Scherf, K. *Chem. Ber.* **1966**, *99*, 3568−3571.
(13) Erhart, M.; Mews, R. *Z. Anorg. Allg. Chem.* **1992**, *615*, 117−122.
(14) Smith, G. L.; Schrobilgen, G. J. *Inorg. Chem.* **2009**, *48*, 7714−7728.
(15) Smith, G. L.; Mercier, H. P. A.; Schrobilgen, G. J. *Inorg. Chem.* **2007**, *46*, 1369−1378.
(16) Mews, R. *J. Chem. Soc., Chem. Commun.* **1979**, *6*, 278−279.
(17) Buss, B.; Clegg, W.; Hartmann, G.; Jones, P. G.; Mews, R.; Noltemeyer, M.; Sheldrick, G. *J. Chem. Soc., Dalton Trans.* **1981**, *1*, 61−63.
(18) Behrens, U.; Hoppenheit, R.; Isenberg, W.; Lork, E.; Petersen, J.; Mews, R. *Z. Naturforsch., B: J. Chem. Sci.* **1994**, *49*, 238−242.
(19) Lork, E.; Petersen, J.; Waterfeld, A.; Mews, R.; Behrens, U. *Z. Anorg. Allg. Chem.* **1997**, *623*, 1518−1524.
(20) Mews, R.; Glemser, O. *Angew. Chem.* **1975**, *87*, 208.
(21) Seppelt, K.; Sundermeyer, W. *Angew. Chem., Int. Ed. Engl.* **1970**, *9*, 905.
(22) Jäckh, C.; Roland, A.; Sundermeyer, W. *Chem. Ber.* **1975**, *108*, 2580−2588.

DOI: 10.1021/acs.inorgchem.5b01769
Inorg. Chem. 2015, 54, 9989−10000

(23) Feser, M.; Höfer, R.; Glemser. *Z. Naturforsch., B: J. Chem. Sci.* **1974**, *29*, 716−718.
(24) Feser, M.; Höfer, R.; Glemser, O. *Z. Naturforsch., B: J. Chem. Sci.* **1975**, *30*, 327−329.
(25) Roland, A.; Sundermeyer, W. *Z. Naturforsch., B: J. Chem. Sci.* **1972**, *27*, 1102−1103.
(26) Höfs, H.; Mews, R.; Noltemeyer, M.; Sheldrick, G. M.; Schmidt, M.; et al. *Z. Naturforsch., B: J. Chem. Sci.* **1983**, *38*, 454−459.
(27) Eisenbarth, R.; Sundermeyer, W. *Angew. Chem.* **1978**, *90*, 226.
(28) Mews, R.; Glemser, O. *J. Chem. Soc., Chem. Commun.* **1973**, *21*, 823−824.
(29) Buss, B.; Altena, D. *Z. Anorg. Allg. Chem.* **1978**, *440*, 65−73.
(30) Buss, B.; Altena, D. Z.; Mews, R.; Glemser, O. *Angew. Chem.* **1978**, *90*, 287−288.
(31) Hoppenheit, R.; Mews, R.; Noltemeyer, M.; Sheldrick, G. M. *Chem. Ber.* **1983**, *116*, 874−881.
(32) Eisenbarth, R.; Sundermeyer, W. *Z. Naturforsch., B: J. Chem. Sci.* **1981**, *36*, 1343−1344.
(33) Eisenbarth, R.; Sundermeyer, W. *Z. Naturforsch., B: J. Chem. Sci.* **1978**, *33*, 1194−1195.
(34) DeBackere, J. R.; Mercier, H. P. A.; Schrobilgen, G. J. *J. Am. Chem. Soc.* **2014**, *136*, 3888−3903.
(35) DeBackere, J. R.; Mercier, H. P. A.; Schrobilgen, G. J. *Inorg. Chem.* **2015**, *54*, 1606−1626.
(36) Huppmann, P.; Hartl, H.; Seppelt, K. *Z. Anorg. Allg. Chem.* **1985**, *524*, 26−32.
(37) Strauss, S. H.; Noirot, M. D.; Anderson, O. P. *Inorg. Chem.* **1985**, *24*, 4307−4311.
(38) Colsman, M. R.; Noirot, M. D.; Miller, M. M.; Anderson, O. P.; Strauss, S. H. *J. Am. Chem. Soc.* **1988**, *110*, 6886−6888.
(39) Colsman, M. R.; Newbound, T. D.; Marshall, L. J.; Noirot, M. D.; Miller, M. M.; Wulfsberg, G. P.; Frye, J. S.; Anderson, O. P.; Strauss, S. H. *J. Am. Chem. Soc.* **1990**, *112*, 2349−2362.
(40) Rack, J. J.; Hurlburt, P. K.; Kellett, P. J.; Luck, J. S.; Anderson, O. P.; Strauss, S. H. *Inorg. Chim. Acta* **1996**, *242*, 71−79.
(41) Hurlburt, P. K.; Anderson, O. P.; Strauss, S. H. *J. Am. Chem. Soc.* **1991**, *113*, 6277−6278.
(42) Newbound, T. D.; Colsman, M. R.; Miller, M. M.; Wulfsberg, G. P.; Anderson, O. P.; Strauss, S. H. *J. Am. Chem. Soc.* **1989**, *111*, 3762−3764.
(43) Smith, G. L.; Mercier, H. P. A.; Schrobilgen, G. J. *J. Am. Chem. Soc.* **2009**, *131*, 7272−7286.
(44) Elgad, U.; Selig, H. *Inorg. Chem.* **1975**, *14*, 140−145.
(45) Bondi, A. *J. Phys. Chem.* **1964**, *68*, 441−451.
(46) Addison, A. W.; Rao, T. N.; et al. *J. Chem. Soc., Dalton Trans.* **1984**, *7*, 1349−1356.
(47) Krebs, B.; Meyer-Hussein, E.; Glemser, O.; Mews, R. *Chem. Commun.* **1968**, *24*, 1578−1579.
(48) Schulz, A.; Villinger, A. *Chem.—Eur. J.* **2015**, *21*, 3649−3663.
(49) Bondi, A. *J. Phys. Chem.* **1966**, *70*, 3006−3007.
(50) Casteel, W. J., Jr.; Dixon, D. A.; Mercier, H. P. A.; Schrobilgen, G. J. *Inorg. Chem.* **1996**, *35*, 4310−4322.
(51) Mews, R.; Keller, K.; Glemser, O. *Inorg. Synth.* **1986**, *24*, 12−17.
(52) Schack, C.; Wilson, R. D. *Inorg. Chem.* **1970**, *9*, 311−314.
(53) Gerken, M.; Dixon, D. A.; Schrobilgen, G. J. *Inorg. Chem.* **2000**, *39*, 4244−4255.
(54) *APEX2*, release v2011.6-1; Bruker AXS, Inc.: Madison, WI, 1995.
(55) Sheldrick, G. M. *SADABS (Siemens Area Detector Absorption Corrections)*, version 2.10; Siemens Analytical X-ray Instruments, Inc.: Madison, WI, 2004.
(56) Sheldrick, G. M. *SHELXTL*, release 6.14; Siemens Analytical X-ray Instruments, Inc.; Madison, WI, 1993−2014.
(57) Spek, A. L. *J. Appl. Crystallogr.* **2003**, *36*, 7−13.
(58) Basis sets were obtained from the Extensible Computational Chemistry Environment Basis set Database, version 2/25/04, as developed and distributed by the Molecular Science Computing Facility, Environmental and Molecular Science Laboratory, which is part of the Pacific Northwest Laboratory, P.O. Box 999, Richland, WA 99352.
(59) Frisch, M. J.; Trucks, G. W.; Schlegel, H. B.; Scuseria, G. E.; Robb, M. A.; Cheeseman, J. R.; Scalmani, G.; Barone, V.; Mennucci, B.; Petersson, G. A.; Nakatsuji, H.; Caricato, M.; Li, X.; Hratchian, H. P.; Izmaylov, A. F.; Bloino, J.; Zheng, G.; Sonnenberg, J. L.; Hada, M.; Ehara, M.; Toyota, K.; Fukuda, R.; Hasegawa, J.; Ishida, M.; Nakajima, T.; Honda, Y.; Kitao, O.; Nakai, H.; Vreven, T.; Montgomery, J. A., Jr.; Peralta, J. E.; Ogliaro, F.; Bearpark, M.; Heyd, J. J.; Brothers, E.; Kudin, K. N.; Staroverov, V. N.; Kobayashi, R.; Normand, J.; Raghavachari, K.; Rendell, A.; Burant, J. C.; Iyengar, S. S.; Tomasi, J.; Cossi, M.; Rega, N.; Millam, N. J.; Klene, M.; Knox, J. E.; Cross, J. B.; Bakken, V.; Adamo, C.; Jaramillo, J.; Gomperts, R.; Stratmann, R. E.; Yazyev, O.; Austin, A. J.; Cammi, R.; Pomelli, C.; Ochterski, J. W.; Martin, R. L.; Morokuma, K.; Zakrzewski, V. G.; Voth, G. A.; Salvador, P.; Dannenberg, J. J.; Dapprich, S.; Daniels, A. D.; Farkas, Ö.; Foresman, J. B.; Ortiz, J. V.; Cioslowski, J.; Fox, D. J. *Gaussian 09*, Revision D.01; Gaussian, Inc: Wallingford, CT, 2009.
(60) NBO 6.0. Glendening, E. D.; Badenhoop, J. K.; Reed, A. E.; Carpenter, J. E.; Bohmann, J. A.; Morales, C. M.; Landis, C. R.; Weinhold, F. Theoretical Chemistry Institute, University of Wisconsin-Madison, 2013.

DOI: 10.1021/acs.inorgchem.5b01769
Inorg. Chem. 2015, 54, 9989−10000